PERGAMON

International Journal of Plasticity 17 (2001) 1351–1366

INTERNATIONAL JOURNAL OF Plasticity

www.elsevier.com/locate/ijplas

# Deformation behavior of tantalum and a tantalum tungsten alloy

Sia Nemat-Nasser *, Rajeev Kapoor [1]

*Center of Excellence for Advanced Materials, University of California, San Diego, La Jolla, CA 92093-0416, USA*

Received in final revised form 11 January 2000

**Abstract**

A comparative study of the deformation behavior of tantalum and a tantalum 2.5 wt.% tungsten alloy is carried out. High strain-rate experimental data are used to develop phenomenological constitutive relations. The temperature and the strain-rate sensitivity of the flow stresses are compared. It is observed that although the flow stress for the Ta–2.5%W alloy is greater than that of Ta, the corresponding temperature and strain-rate sensitivity is less pronounced. Ta–2.5%W experiences a solid-solution softening, wherein the athermal stress component has increased, while the thermal component has decreased by the alloying.


## 1. Introduction

The addition of solute atoms in small quantities can sometimes result in a decrease of the yield stress, commonly referred to as solid-solution softening (Mitchell and Raffo, 1967; Das and Arsenault, 1968; Smialek et al., 1970; Christian, 1983). In the case where the flow stress is considered as a sum of a thermal and an athermal component, the solute atoms can have a different effect on each component. The athermal component generally increases with alloying. It is the thermal component which actually experiences the softening effect. In the case where only the thermal component decreases with solute addition, the softening is referred to as pseudo-softening. A prerequisite for pseudo-softening is that the temperature sensitivity of the flow stress decreases with alloying (Pink and Arsenault, 1978). Ta–W (Das and Arsenault, 1968; Gourdin et al., 1994), and Ta–Re (Mitchell and Raffo, 1967), and Ta–Nb (Arsenault, 1966) alloys do show such substitutional alloy softening. Das

* Corresponding author. Tel.: +1-858-534-4914; fax: +1-858-534-2727.
*E-mail address:* sia@shiba.ucsd.edu (S. Nemat-Nasser).
[1] Formally with the Center of Excellence for Advanced Materials, University of California, San Diego, presently as scientist at Materials Science Division, Bhabha Atomic Research Centre, Mumbai 400085, India.

0749-6419/00/$ - see front matter 
PII: S0749-6419(00)00088-7

and Arsenault (1968) showed that the athermal stress component increases with increasing W additions to Ta, whereas the thermal component first decreases and then increases with an increasing alloying element. The activation energy for the slip changes with alloying, being 1.1, 0.9 and 1.3 eV for Ta–2 at. %W, and Ta–9 at.%W, respectively. Gourdin et al. (1994) observed a decrease in the strain-rate sensitivity of the flow stress in Ta with the addition of W. They speculated that in both Ta and the Ta–W alloy, the Peierls mechanism as well as the dislocation obstacle mechanism are operative. Initial deformation is controlled by the Peierls mechanism and at higher strains the obstacle mechanism takes over. Arsenault (1966) investigated the dependence of the activation energies on alloying Ta with Nb, and Ta with W. The addition of 9.2 at.% Nb decreased the activation energy, whereas the addition of W did not change the activation energy. The addition of Nb increased the athermal stress component, but decreased the thermal stress component.

Presented here are experimental results for tantalum and tantalum–2.5 wt.% tungsten alloy. The experimental results are used to develop a physically-based constitutive relation for the flow stress, and the corresponding constitutive parameters for Ta and Ta–2.5%W are compared. The flow stress, and the temperature and strain-rate sensitivities of the flow stress of these materials are also compared. The reader interested in other models and related experimental results, and references, is referred to a recent review article by Liang and Khan (1999).

## 2. Experiments

Commercially pure Ta and Ta–2.5%W are obtained in the form of disks from US Army Ardec. The material is originally in the form of bars. These are cold-upset forged, annealed and high energy-rate formed to a liner, roughly 5 mm high, and then annealed. The grain size is observed to be about 85 μm for Ta, and about 45 μm for Ta–2.5%W. The major impurities present in Ta are C∼10 ppm, O∼60 ppm, N∼10 ppm, Si∼10 ppm, and Nb∼60 ppm, while those present in Ta–2.5%W are C∼10 ppm, O∼53 ppm, N∼10 ppm, and Nb∼330 ppm. Of these only C, O, N, and Si are in the interstitial form, whereas Nb is in the substitutional form. Compression tests are carried out at strain rates ranging from $10^{-4}$/s to 3000/s, and temperatures ranging from 296 to 1000 K. High strain rates of 3000/s are achieved using a split Hopkinson pressure bar with a momentum trap (Nemat-Nasser et al., 1991). High-temperature tests at high strain rates are carried out using a modified Hopkinson bar such that minimal heating of the incident and transmission bars takes place (Nemat-Nasser and Isaacs, 1997).

## 3. Results

### 3.1. Physically-based constitutive modeling

In many cases the shear resistance that a dislocation experiences during glide on a slip plane can be represented as a sum of an athermal part, $\tau_a$, and a thermal part, $\tau^*$.

The athermal resistance in turn can be represented as a sum of two components, that which evolves with deformation ($\tau_{a1}$), and that which remains constant with deformation ($\tau_{a2}$). If the parameter describing the microstructure is represented as $S$, then

$$\tau(S, \dot{\gamma}, T) = \tau_{a2} + \tau_{a1}(S) + \tau^*(\dot{\gamma}, T). \tag{1}$$

The model presented here is a combination of the models proposed by Follansbee and Kocks (1988) and Follansbee et al. (1990), and that of Nemat-Nasser and Isaacs (1997) and Nemat-Nasser et al. (1998). Here a brief description is given. For a more complete analysis of such constitutive modeling, see the above citations. In order to obtain a relation among the shear strain rate, $\dot{\gamma}$, the temperature, $T$, and the thermal shear stress component, $\tau^*$, a relation between $\Delta G$ (the activation free energy for overcoming a short-range barrier), and $\tau^*$ is required. Kocks et al. (1975) suggest an empirical relation between $\Delta G$ and $\tau^*$, representing a typical barrier encountered by a dislocation,

$$\Delta G = F_0\left[1 - \left(\frac{\tau^*}{\hat{\tau}^*}\right)^p\right]^q \tag{2}$$

where $0 < p \leqslant 1$ and $1 \leqslant q \leqslant 2$. Here $\hat{\tau}^*$ is the shear stress required to overcome the barrier at 0 K, and $F_0$ is the free energy required to overcome the barrier when the applied $\tau^*$ is zero. $\dot{\gamma}$ is related to $\Delta G$ as,

$$\dot{\gamma} = \dot{\gamma}_0 \exp\left(-\frac{\Delta G}{kT}\right), \tag{3}$$

where $\dot{\gamma}_0 = \rho_m bav$, $\rho_m$ is the mobile dislocation density, $b$ is the Burgers vector, $a$ is the distance the dislocation moves while overcoming the obstacle, and $v$ is the frequency factor relating to atomic jumps. Putting Eqs. (3) in (2) and simplifying, obtain

$$\tau^* = \hat{\tau}^*\left[1 - \left(\frac{kT}{F_0}\ln\frac{\dot{\gamma}_0}{\dot{\gamma}}\right)^{1/q}\right]^{1/p}. \tag{4}$$

By adding $\tau_a$ to $\tau^*$, the total shear stress can be written as,

$$\tau = \tau_{a1}(S) + \tau_{a2} + \hat{\tau}^*\left[1 - \left(\frac{kT}{F_0}\ln\frac{\dot{\gamma}_0}{\dot{\gamma}}\right)^{1/q}\right]^{1/p}. \tag{5}$$

In the above analysis, shear stress $\tau$ and shear strain rate $\dot{\gamma}$ are used. Here it is assumed that the corresponding macroscopic quantities, the uniaxial stress $\sigma$, and the macroscopic strain rate $\dot{\varepsilon}$, can be averaged such that they relate to each other in a manner similar to Eq. (5). In this particular case, it is assumed that the short-range

barrier does not depend on the dislocation microstructure. Further, if the evolution of the structure parameter ($S$) does not depend on the applied strain rate and temperature, the athermal component depends on the current structure which changes only by the change in the dislocation density and distribution. This change may be represented *empirically* by the extent of deformation, i.e. the strain, although the plastic strain is not a state variable. Thus the constitutive equation relating the stress, strain, strain rate, and temperature, can be written as,

$$\sigma = \sigma_{a1}(\varepsilon) + \sigma_{a2} + \hat{\sigma}^* \left[ 1 - \left( \frac{kT}{F_0} \ln \frac{\dot{\varepsilon}_0}{\dot{\varepsilon}} \right)^{1/q} \right]^{1/p}, \tag{6}$$

where ε is the uniaxial strain. There exists an inherent temperature dependence in the flow stress, that of the temperature dependence of the shear modulus, $\mu(T)$ ($\sigma_{a1} \propto \mu(T)$, $\sigma_{a2} \propto \mu(T)$ and $\hat{\sigma}^* \propto \mu(T)$). $\hat{\sigma}^*$ is the value of $\sigma^*$ at 0 K, also called the mechanical threshold stress (Follansbee and Kocks, 1988; Follansbee et al., 1990). The shear modulus, $\mu$, has a temperature dependence of the form (Varshni, 1970)

$$\frac{\mu(T)}{\mu_0} = 1 - \frac{c_1}{\exp \frac{c_2}{T} - 1} = f(T), \tag{7}$$

where $c_1$ and $c_2$ are constants determined by fitting Eq. (7) to the shear modulus–temperature data (Simmons and Wang, 1971). Thus, to obtain a temperature-dependent part of the flow stress without taking into account the dependence of the shear modulus on the temperature, $\sigma/f(T)$ instead of $\sigma$, should be considered. The values of $p$ and $q$ in Eq. (6) are such that $0 < p \leqslant 1$ and $1 \leqslant q \leqslant 2$. Ono (1968) suggests that many predicted barrier shapes fit a straight line for a $\sigma^{*1/2}$ vs. $T^{2/3}$ plot, which translates to $p = 1/2$ and $q = 3/2$. In previous studies (Nemat-Nasser and Isaacs, 1997; Nemat-Nasser et al., 1998) $p = 2/3$ and $q = 2$ have been used to fit experimental data obtained by deforming polycrystalline tantalum at 5000/s. Choosing either $p = 1/2$ and $q = 3/2$, or $p = 2/3$ and $q = 2$ does not significantly change the barrier profile, and either set of values can be used to fit the experimental data. The present experimental results produced a better fit if $p$ and $q$ are chosen as $p = 1/2$ and $q = 3/2$. Using these values of $p$ and $q$, $\sigma^*$ [last part of Eq. (6)], is expressed as,

$$\sigma^* = \hat{\sigma}^* \left[ 1 - \left( \frac{kT}{F_0} \ln \frac{\dot{\varepsilon}_0}{\dot{\varepsilon}} \right)^{2/3} \right]^2. \tag{8}$$

Thus, from Eq. (8), a plot of $[\sigma^*/f(T)]^{1/2}$ vs. $T^{2/3}$ should produce a straight line, with

$$\text{intercept} = \sqrt{\frac{\hat{\sigma}^*}{f(T)}} \quad \text{and} \quad \text{slope} = -\left( \frac{k}{F_0} \ln \frac{\dot{\varepsilon}_0}{\dot{\varepsilon}} \right)^{2/3} \sqrt{\frac{\hat{\sigma}^*}{f(T)}}. \tag{9}$$

The normalized athermal component, $\sigma_a/f(T)$, (the regime where the flow stress is independent of temperature) is determined from a plot of $\sigma/f(T)$ vs. $T$. This value is subtracted from $\sigma/f(T)$ to obtain $\sigma^*/f(T)$.

### 3.2. Fit of constitutive equation to experimental results

Fig. 1(a) is the stress–strain plot for Ta tested at 3000/s, at various indicated initial temperatures. Fig. 1(b) is a plot of the flow stress as a function of temperature, at different strains, as obtained from Fig. 1(a). The flow stress decreases with an increase in the temperature up to a point where the flow stress becomes independent of the temperature. It is assumed that when $\sigma/f(T)$ becomes independent of $T$, it represents the athermal stress component, $\sigma_a/f(T)$. This value ($\sigma_a/f(T)$) can be subtracted from the overall stress, $\sigma^*/f(T)$ to obtain the thermal component of the stress, $\sigma^*/f(T)$. As seen in Fig. 1(c), values of $\sigma^*/f(T)$ at different strains fall on essentially a common curve, suggesting that in this strain rate and temperature range, the normalized thermal stress does not depend on the strain.

Fig. 2(a) is the stress–strain plot for Ta–2.5%W tested at various indicated initial temperatures. Fig. 2(b) is a plot of the flow stress as a function of temperature, at different strains, as obtained from Fig. 2(a). As for the case of Ta, here too the value of $\sigma_a/f(T)$ is subtracted from $\sigma/f(T)$ to obtain $\sigma^*/f(T)$. Fig. 2(c) is a plot of $\sigma^*/f(T)$ vs. $T$ at different strains. As for Ta, for Ta–2.5%W too, $\sigma^*/f(T)$ does not depend on the strain. Values of $\sigma^*/f(T)$ for different strains appear to lie on a common curve, although not as neatly as in the case of Ta. This validates the earlier assumption that the athermal stress depends only on the microstructure, whereas the thermal stress depends only on the strain rate and temperature.

Fig. 3 is a plot of the normalized flow stress $\sigma/f(T)$ at 0.05 strain vs.\ temperature for Ta and Ta–2.5%W. Ta–2.5%W has a higher overall flow stress as compared to Ta, but the temperature sensitivity of the flow stress is lower than that of Ta. It would be interesting to compare the height of the thermal barrier, $\hat{\sigma}^*$, for Ta and Ta–2.5%W. Physically, $\hat{\sigma}^*$ represents the height of the thermal barrier at 0 K. From the data in Fig. 3 we subtract the athermal contributions for Ta and Ta–2.5%W, respectively, to obtain the thermal stress contributions. This is then plotted as $[\sigma^*/f(T)]^{1/2}$ vs. $T^{2/3}$ for Ta and Ta–2.5%W, as shown in Fig. 4(a) and (b) respectively. Shown in the plots are the equation of the fit, and the goodness of the fit,[1] $R$. The experimental points fit a straight line with intercepts 33.76 for Ta, and 27.67 for Ta–2.5%W. Using Eq. (9) obtain,

$$\hat{\sigma}^* = 1140 \quad \text{MPa for Ta,}$$
$$\text{and } \hat{\sigma}^* = 7.65\,\text{MPa for Ta}-2.5\%\text{W.}$$

[1] Here, the goodness of the fit is defined by,

$$R = \frac{n\sum(x_i y_i) - \left(\sum x_i\right)\left(\sum y_i\right)}{\sqrt{\left|n\sum x_i^2 - \left(\sum x_i\right)^2 \left\| n\sum y_i^2 - \left(\sum y_i\right)^2\right|}},$$

where $n$ is the number of data points, and $x_i$ and $y_i$ are the data points.

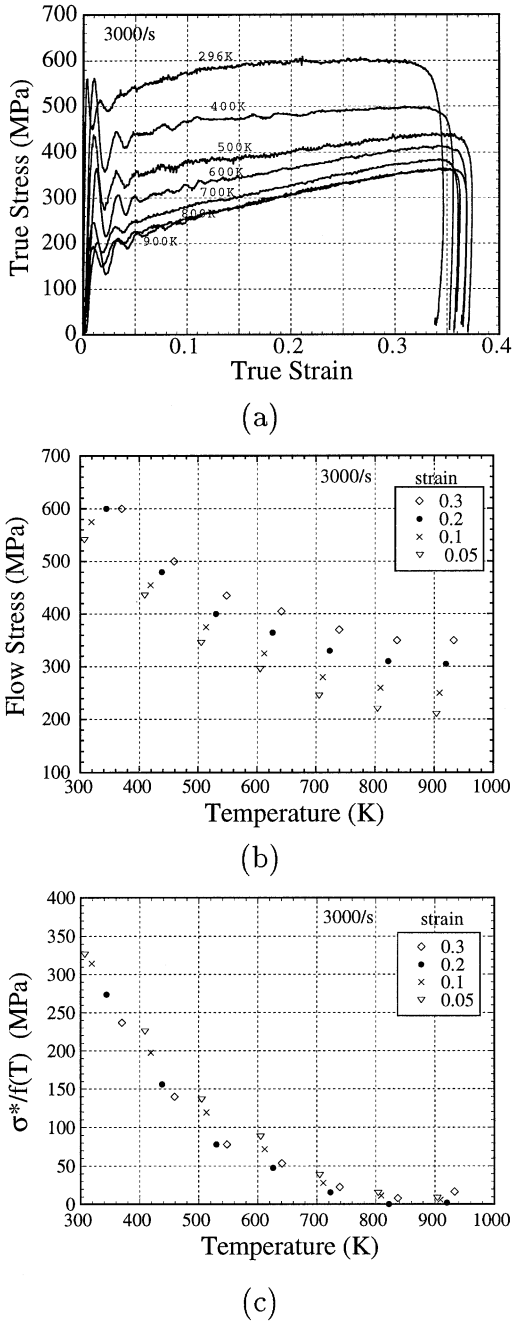


Fig. 1. (a) Flow stress curves for Ta deformed at 3000/s; (b) flow stress for Ta as function of temperature at different strains; and (c) $\sigma^*/f(T)$ as function of $T$ for different strains.

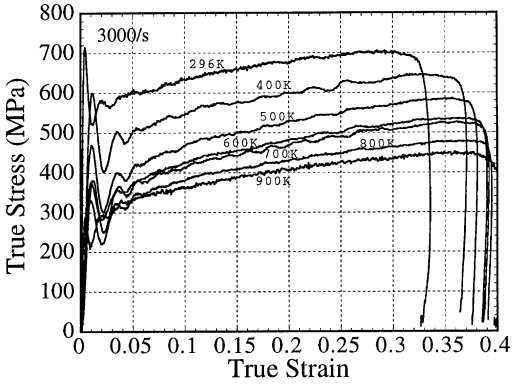


(a)

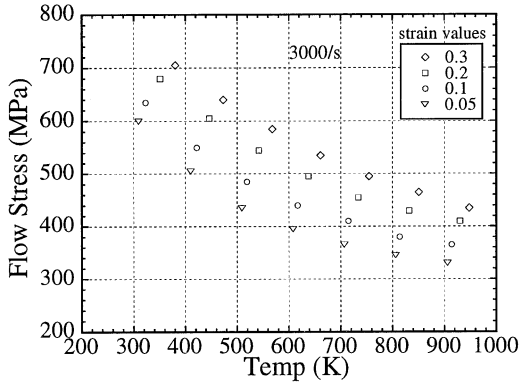


(b)

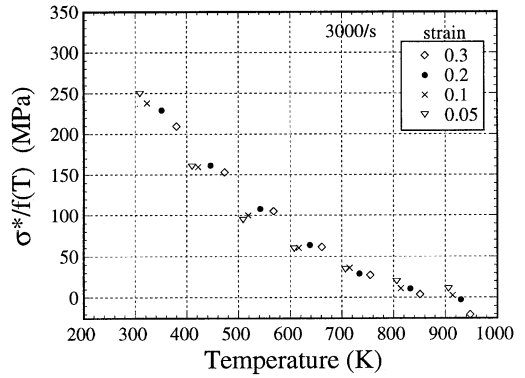


(c)

Fig. 2. (a) Flow stress curves for Ta–2.5%W deformed at 3000/s; (b) flow stress for Ta–2.5%W as a function of temprature at different strains; and (c) $\sigma^*/f(T)$ as function of temperature for different strain values.

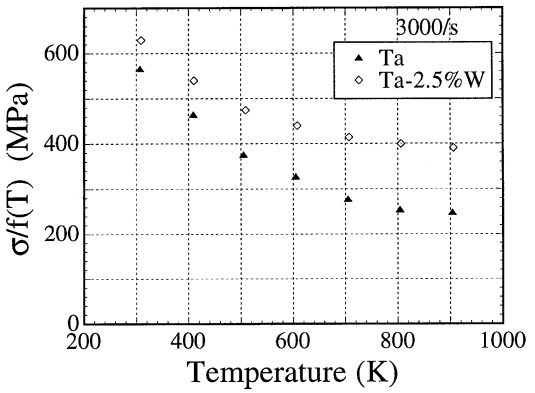


Fig. 3. Plot of $\sigma/f(T)$ vs. $T$ at 0.05 strain at 3000/s for Ta and Ta–2.5%W.

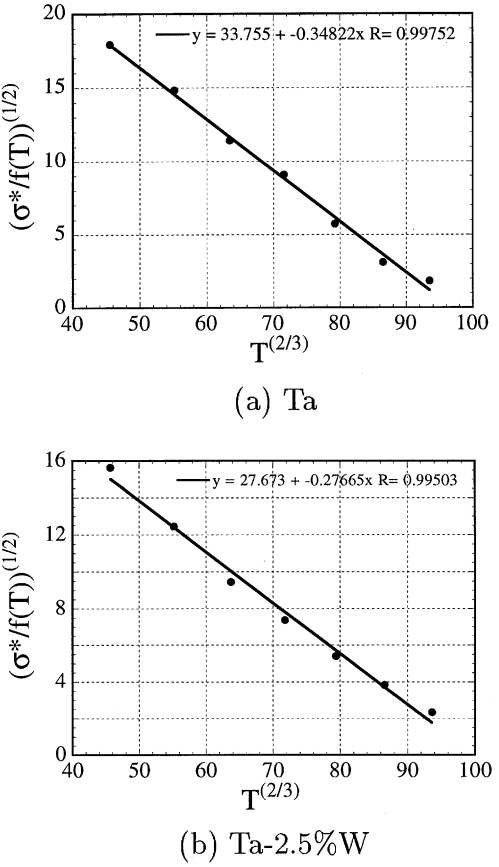


Fig. 4. Plot of $\sqrt{\sigma^*/f(T)}$ vs. $T^{2/3}$ for (a) Ta, and (b) Ta–2.5%W.

The temperature at which $\sigma^* = 0$, called $T_c$, is obtained from the intercept of the straight lines with the x-axis in Fig. 4. From this

$$T_c = 954\text{K for Ta},$$

and $T_c = 1000\,\text{K}$ for Ta−2.5%W.

For Ta, the $y$-axis intercept of the $[\sigma^*/f(T)]^{1/2}$ vs. $T^{2/3}$ plot is −0.3482. Thus from Eq. (9),

$$\left(\frac{k}{F_0}\ln\frac{\dot{\varepsilon}_0}{\dot{\varepsilon}}\right)^{2/3}\sqrt{\frac{\hat{\sigma}^*}{f(T)}} = 0.3482, \tag{10}$$

$$\frac{k}{F_0}\ln\left(\frac{\dot{\varepsilon}_0}{\dot{\varepsilon}}\right) = \left(\frac{0.3482}{33.76}\right)^{3/2} = 1.05\times10^{-3}. \tag{11}$$

If $F_0 = 1$ eV, and with $k = 8.63\times10^{-5}$ eV/K, then $\dot{\varepsilon}_0 = 5\times10^8$/s. The normalized thermal stress component can now be written as,

$$\frac{\sigma^*}{f(T)} = 1140\left[1-\left\{\frac{kT}{1.0}\ln\left(\frac{5\times10^8}{\dot{\varepsilon}}\right)\right\}^{2/3}\right]^2. \tag{12}$$

For Ta–2.5%W, the $y$-axis intercept of the $[\sigma^*/f(T)]^{1/2}$ vs. $T^{2/3}$ plot is −0.2767. Thus,

$$\left(\frac{k}{F_0}\ln\frac{\dot{\varepsilon}_0}{\dot{\varepsilon}}\right)^{2/3}\sqrt{\frac{\hat{\sigma}^*}{f(T)}} = 0.2767, \tag{13}$$

$$\frac{k}{F_0}\ln\left(\frac{\dot{\varepsilon}_0}{\dot{\varepsilon}}\right) = \left(\frac{0.2767}{27.67}\right)^{3/2} = 1.0\times10^{-3}. \tag{14}$$

If $F_0 = 1$ eV, then $\dot{\varepsilon}_0 = 3.2\times10^8$/s. The normalised thermal stress component for Ta–2.5%W can now be written as,

$$\frac{\sigma^*}{f(T)} = 765\left[1-\left\{\frac{kT}{1.0}\ln\left(\frac{3.2\times10^8}{\dot{\varepsilon}}\right)\right\}^{2/3}\right]^2. \tag{15}$$

Recall that $\dot{\varepsilon}_0 = C\rho_m bav$, where $C$ is the converting factor from the microscopic quantities listed to the macroscopic reference strain rate, $\rho_m$ is the mobile dislocation density, $b$ is the Burgers vector, and $a$ is the distance the dislocation moves while overcoming the short-range obstacle. During deformation, the only parameters

which can change are $\rho_m$, the mobile dislocation density, and $a$, the distance between the short-range obstacles. From the above experimental observation, $\dot{\varepsilon}_0$ has decreased with the addition of W to Ta, implying that either $\rho_m$ or $a$ has decreased. Since the reference strain rate, $\dot{\varepsilon}_0$, and the activation free energy $F_0$ are coupled together in one term, a plot of the type $[\sigma^*/f(T)]^{1/2}$vs. $T^{2/3}$ is unable to determine these parameters separately. Here, it is assumed that $F_0$ is 1 eV, and then $\dot{\varepsilon}_0$ is determined. Conversely, a reasonable value for $\dot{\varepsilon}_0$ could be assumed, and then $F_0$ can be determined.

The next step in this constitutive modeling is to calculate the athermal stress component as a function of the microstructural parameters. We assume that these parameters may be represented by the average dislocation density, and that this density is a function of the strain (which is a monotonically increasing parameter, for positive strain rates). Hence, the athermal stress may be assumed to depend on the strain (which is here used as an independent variable, and not as a structural parameter). From the plot of $\sigma/f(T)$ vs. (Fig. 3), it is seen that at temperatures of 900 K and higher, the stress can be considered as athermal. Thus, putting $\sigma^* = 0$ in Eq. (6), the stress–strain curve at 900 K is fitted to a power law equation of the form

$$\frac{\sigma_a}{f(T)} = \frac{\hat{\sigma}_{a1}}{f(T)}\varepsilon^n + \frac{\sigma_{a2}}{f(T)}. \tag{16}$$

Fig. 5(a) and (b) shows the stress–strain relations at 900 K and 3000/s fitted to Eq. (16) for Ta and Ta–2.5%W, respectively. In Table 1, the parameters for the following final constitutive equation for Ta and Ta–2.5%W are compared,

$$\frac{\sigma}{f(T)} = \frac{\hat{\sigma}_{a1}}{f(T)}\varepsilon^n + \frac{\sigma_{a2}}{f(T)} + \frac{\hat{\sigma}^*}{f(T)}\left[1 - \left(\frac{kT}{F_0}\ln\frac{\dot{\varepsilon}_0}{\dot{\varepsilon}}\right)^{1/2}\right]^{3/2}. \tag{17}$$

Putting the parameters listed in Table 1 into Eq. (17), the stress–strain curves at different temperatures are calculated. These calculated curves are compared to the corresponding experimental data, as shown in Fig. 6. The calculated curves do follow the trend of the experimental data for both Ta and Ta–2.5%W.

The steps to obtain the constitutive equation are as follows:

1. Normalize the measured flow stress with the temperature-dependent shear modulus.
2. Plot the normalized flow stress, $\sigma/f(T)$, vs. $T$. From this plot estimate $\sigma_a/f(T)$ at the point it becomes independent of the temperature.
3. Obtain the thermal stress values using $\dfrac{\sigma^*}{f(T)} = \dfrac{\sigma}{f(T)} - \dfrac{\sigma_a}{f(T)}$.
4. Plot $[\sigma^*/f(T)]^{1/2}$ vs. $T^{2/3}$ to obtain a straight line with

$$\text{intercept} = \sqrt{\frac{\hat{\sigma}^*}{f(T)}} \text{ and slope} = -\left(\frac{k}{F_0}\ln\frac{\dot{\varepsilon}_0}{\dot{\varepsilon}}\right)^{2/3}\sqrt{\frac{\hat{\sigma}*}{f(T)}}.$$

5. To obtain the athermal component, consider the stress–strain curve at such a temperature where the temperature sensitivity of the flow stress is zero. This $\sigma/f(T)$ vs. $\varepsilon$ curve is fitted to Eq. (16).
6. The athermal stress component and the thermal stress component are added and the effect of the shear modulus reintroduced,

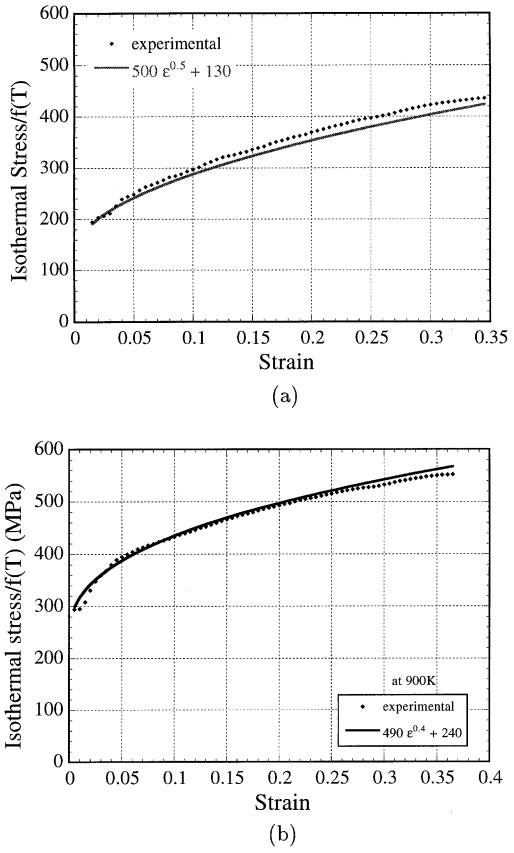


Fig. 5. Isothermal flow stress of (a) Ta and (b) Ta–2.5%W, at 900 K–3000/s, fitted to Eq. [16]. Here, it is assumed that the flow stress at 900 K–3000/s is athermal.

Table 1
List of the parameters of Eq. (17) as applied to high strain-rate experimental results of Ta and Ta–2.5%W

| | Ta | Ta–2.5%W |
|---|---|---|
| $\hat{\sigma}^*/f(T)$ | 1140 MPa | 765 MPa |
| $\dot{\varepsilon}_0$ | $5\times10^8$/s | $3.2\times10^8$/s |
| $\hat{\sigma}_{a1}/f(T)$ | 500 MPa | 490 MPa |
| n | 0.5 | 0.4 |
| $\sigma_{a2}/f(T)$ | 130 MPa | 240 MPa |

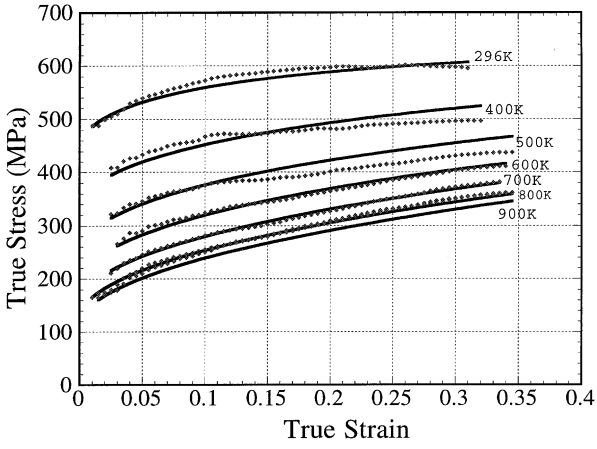


(a) Ta at 3,000/s.

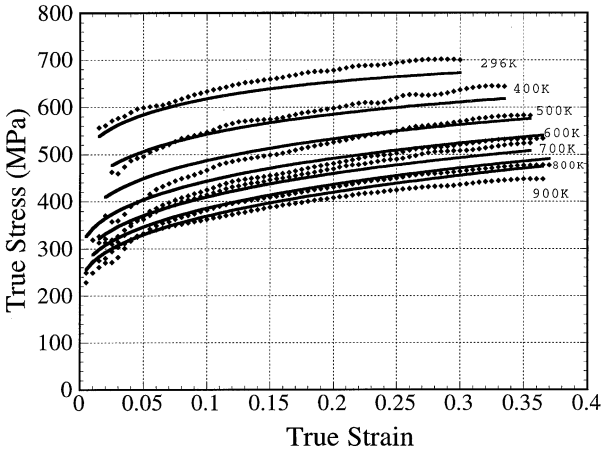


(b) Ta-2.5%W at 3,000/s.

Fig. 6. Experimental flow stress as function of strain, compared to calculated values using Eq. (17).

$$\sigma = \left(\sigma_{a2} + \hat{\sigma}_{a1}\varepsilon^n + \hat{\sigma}^*\left[1 - \left\{\frac{kT}{F_0}\ln\left(\frac{\dot{\varepsilon}_0}{\dot{\varepsilon}}\right)\right\}^{2/3}\right]^2\right)\left(1 - \frac{c_1}{\exp\frac{c_2}{T} - 1}\right). \tag{18}$$

The above procedure for obtaining a constitutive equation does not take into account the microstructural evolution. Eq. (18) is valid if (1) the work-hardening rate does not depend on the applied strain rate and the testing temperature, (2) the thermal component of the stress does not change with deformation, and (3) the microstructure can be empirically represented by the strain (which is *not* a state

variable). In the present set of experiments carried out on Ta and Ta–2.5%W, these assumptions seem to hold for monotonic deformations at high strain-rates (3000/s) and temperatures ranging from 296 to 1000 K. During low-strain rate tests, dynamic strain aging occurs, making the work-hardening rate dependent on the applied strain rate and the testing temperature.

### 3.3. Comparison between Ta and Ta–2.5%W

The addition of 2.5 wt.% tungsten to tantalum leads to an increase in the overall flow stress for all strain rates and temperatures. Comparisons between the stress–strain curves of Ta and Ta–2.5%W at (a) 296 K-3000/s, (b) 296 K-0.01/s, (c) 296 K-0.0001/s, and (d) 1000 K-0.01/s, are shown in Fig. 7. For each of the low strain-rate tests, the initial work-hardening rate is higher for Ta–2.5%W than it is for Ta. At 3000/s-296 K, the combined work-hardening rate (work-hardening rate and temperature softening due to adiabatic heating) is greater for Ta–2.5% than for Ta. Fig. 8 includes plots of $\sigma^*/f(T)$ vs. $T$ at 3000, 500, 0.1, and 0.01/s respectively, for both materials. Data points are joined by straight lines only for clarity, and do not indicate any interpolation trends. At 3000/s [Fig. 8(a)], the temperature sensitivity of the flow stress is clearly smaller for Ta–2.5%W than it is for Ta. Reduced temperature sensitivity for Ta–2.5%W is also observed at lower strain rates of 500, 0.1 and 0.01/s, although it is not as clear as it is for 3000/s. At a strain rate of 0.01/s, both Ta and Ta–2.5%W show dynamic strain aging near a temperature of 650–700 K. In

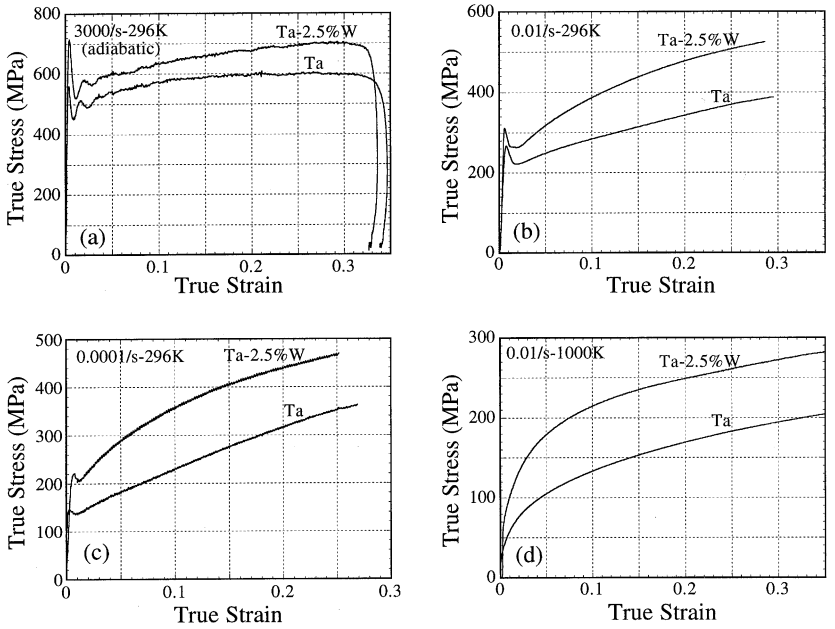


Fig. 7. Stress–strain plot, comparing Ta and Ta–2.5%W at (a) 3000/s–296 K, (b) 0.01/s–296 K, (c) 0.0001/s–296 K, and (d) 0.01/s–1000 K.

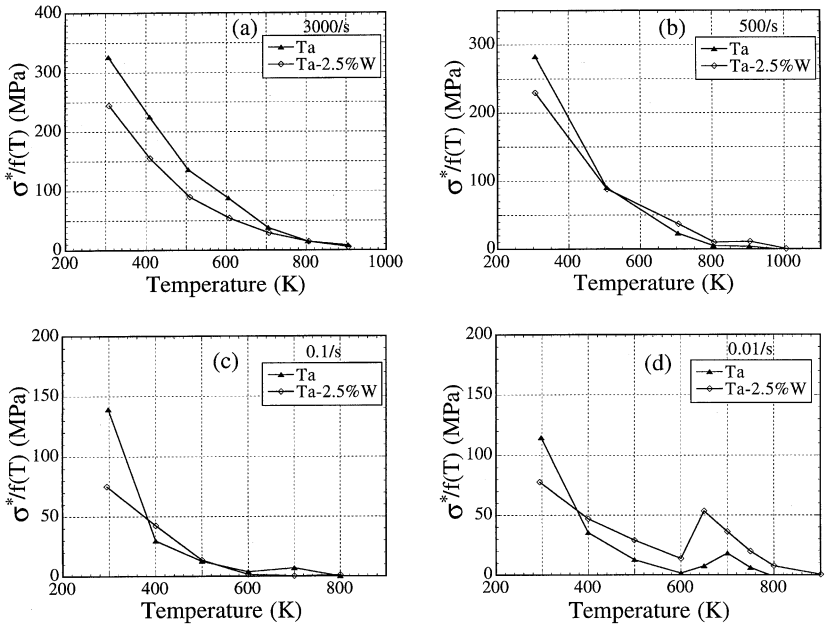


Fig. 8. Flow stress as a function of temperature, comparing Ta and Ta–2.5%W at (a) 3000/s, (b) 500/s, (c) 0.1/s, and (d) 0.01/s.

Fig. 9 plots of $\sigma/f(T)$ vs. $\log(\dot{\varepsilon})$ are shown for Ta and Ta–2.5%W, at 77, 296, 500 and 800 K. At 77 Kthe strain-rate sensitivities are similar for Ta and Ta–2.5%W. At 296, 500 and 800 K, and at a lower strain rate, the strain-rate sensitivity is smaller for Ta–2.5%W than it is for Ta. At higher strain rates, the strain-rate sensitivity is greater for Ta–2.5%W than it is for Ta. As observed in Table 1, the athermal stress component (the part not dependent on deformation, $\sigma_{a2}$) is greater for Ta–2.5%W. The thermal stress component has a smaller temperature dependence for Ta–2.5%W, as is seen through the value of $\hat{\sigma}^*$. Thus, it is observed that the addition of tungsten to tantalum reduces the temperature sensitivity of the stress. On the other hand, it does increase the overall stress, and results in a higher work-hardening rate. Solution softening can be explained by either an extrinsic or an intrinsic mechanism. The extrinsic mechanism suggests that, added solutes interact with already existing impurities (interstitial elements) to form complexes, and thereby reducing the pre-existing hardening effects that the interstitials cause (Smialek et al. 1970). Some intrinsic theories suggest an enhancement of the thermally activated nucleation rate of double kink formation by affecting the core of the dislocation and the Peierls stress (Sato and Meshii, 1973; Arsenault and de Wit, 1974; Arsenault and Cadman, 1980; Easterling and Arsenault, 1982). In the present set of experiments, dynamic strain aging is observed for both Ta and the Ta–2.5%W alloy, suggesting that the interstitial impurities are not effectively removed by the W atoms. Thus, it is likely that solid-solution softening is caused by intrinsic mechanisms. The short-range barriers become shorter but flatter, such that, although the barrier height ($\hat{\sigma}^*$)

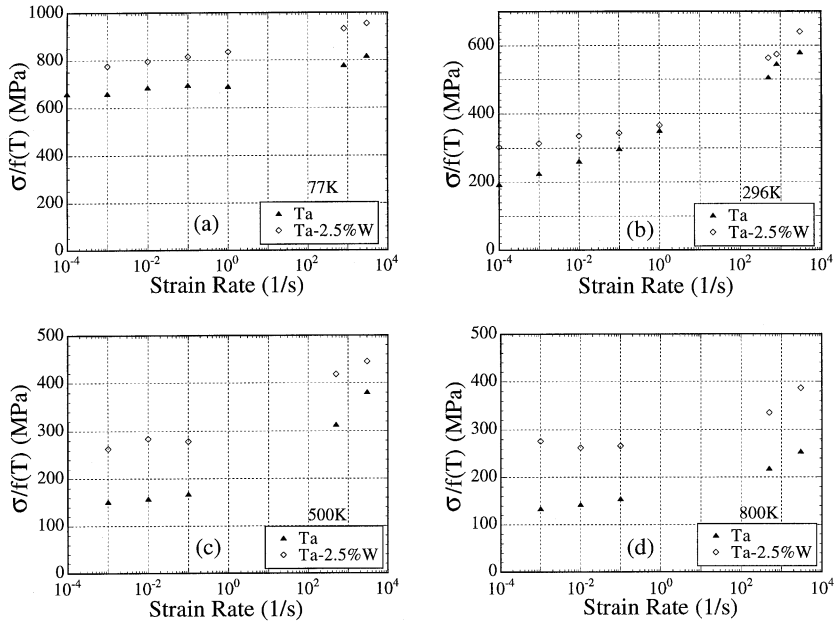


Fig. 9. Flow stress as a function of strain rate, comparing Ta and Ta–2.5%W at (a) 77 K, (b) 296 K, (c) 500 K and (d) 800 K.

decreases, the critical temperature, $T_c$, required for overcoming short-range barriers by thermal activation, increases.

## 4. Conclusions

An attempt is made to apply a simple one-term thermal-activation theory to explain the strain-rate and temperature dependence of the flow stress at high strain rates, for Ta and Ta–2.5%W. At low strain rates and high temperatures, dynamic strain aging effects are observed. Although the overall flow stress increases with the addition of tungsten, the temperature and the strain-rate sensitivity of the flow stress decrease. The height of the thermal barrier, which is measured as the thermal stress component at 0 K, also decreases with the alloying of tungsten to tantalum. However, the temperature at which the thermal energy is sufficient for overcoming the short-range barriers, increases with alloying. Overall, the addition of 2.5 wt.% tungsten to tantalum results in pseudo-solid-solution softening.

## Acknowledgements

This work was supported by the US Army Research Office (ARO) Contract ARO DAAL 03-92-G-0108 to the University of California, San Diego.

## References

Arsenault, R.J., 1966. An investigation of the mechanism of thermally activated deformation in Ta and Ta based alloys. Acta Metallurgica 14, 831–838.

Arsenault, R.J., Cadman, T.W., 1980. The effect of impurity interstitials on the lattice resistance to dislocation motion. Metallurgical Transactions 11A, 127–134.

Arsenault, R.J., de Wit, R., 1974. Distributed glide force between a non-spherical defect and a dislocation. Acta Metallurgica 22, 819–827.

Christian, J.W., 1983. Some surprising features of the plastic deformation of bcc metals and alloys. Metallurgical Transactions A 14A, 1237–1256.

Das, G.S., Arsenault, R.J., 1968. Non-monotonic strengthening in bcc solid solutions. Scripta Metallurgica 2, 495–500.

Easterling, D.M., Arsenault, R.J., 1982. Peierls-Nabarro plastic deformation in the presence of solute clusters. Metallurgical Transactions A 13A, 1429–1434.

Follansbee, P.S., Kocks, U.F., 1988. A constitutive description of the deformation of copper based on the use of the mechanical threshold stress as an internal state variable. Acta Metallurgica 36 (1), 81–93.

Follansbee, P.S., Huang, J.C., Gray, G.T., 1990. Low-temperature and high strain rate deformation of nickel and nickel-carbon alloys and analysis of the constitutive behavior according to an internal state variable model. Acta Metallurgica et Materialia 38 (7), 1241–1254.

Gourdin, W.H., Lassila, D.H., Leblanc, M.M., Shields, A.L., 1994. The influence of tungsten alloying on the mechanical properties of Tantalum. Journal De Physique IV 4 (C8), 207–212.

Kocks, U.F., Argon, A.S., Ashby, M.F., 1975. Thermodynamics and kinetics of slip. Progress in Materials Science 19, 231–271.

Liang, R., Khan, A.S., 1999. critical review of experimental results and constitutive models for bcc and fcc metals over a wide range of strain rates and temperatures. International Journal of Plasticity 15, 963–980.

Mitchell, T.E., Raffo, P.L., 1967. Mechanical properties of some Tantalum alloys. Canadian Journals of Physics 45, 1047–1062.

Nemat-Nasser, S., Isaacs, J.B., 1997. Direct measurement of isothermal flow stress of metals at elevated temperatures and high strain rates with application to Ta and Ta-W alloys. Acta Materialia 45 (3), 907–919.

Nemat-Nasser, S., Isaacs, J.B., Starrett, J.E., 1991. Hopkinson techniques for dynamic recovery experiments. Proceedings of the Royal Society of London A 435, 371.

Nemat-Nasser, S., Okinaka, T., Ni, L., 1998. A physically based constitutive model for bcc crystals with application to polycrystalline tantalum. Journal of Mechanics and Physics of Solids 46 (6), 1009–1038.

Ono, K., 1968. Temperature dependence of dispersed barrier hardening. Journal of Applied Physics 39 (3), 1803–1806.

Pink, E., Arsenault, R.J., 1978. Low-temperature softening in body-centered cubic alloys. Progress in Materials Science 24, 1–50.

Sato, A., Meshii, M., 1973. Solid solution softening and solution hardening. Acta Metallurgica 21, 753–768.

Simmons, G. and Wang, H., 1971. Single Crystal Elastic Constants and Calculated Aggregate Properties: A Handbook., 2nd Edition. The M.I.T. Press.

Smialek, R.L., Webb, G.L., Mitchell, T.E., 1970. Solid solution softening in bcc metals alloys. Scripta Metallurgica 4, 33–38.

Varshni, Y.P., 1970. Temperature dependence of the elastic constants. Physical Review B 2 (10), 3952–3958.